Journal of Materials Chemistry C

Accepted Manuscript

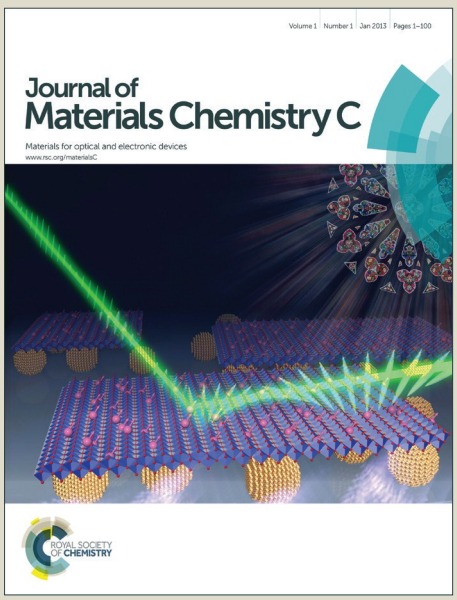

ROYAL SOCIETY OF CHEMISTRY

www.rsc.org/materialsC

Journal of Materials Chemistry C

RSCPublishing

ARTICLE

Facile Fabrication of Color-Tunable and White Light Emitting Nano-Composite Films Based on Layered Rare-earth Hydroxides

Liangliang Liu,[a] Minghui Yu,[a] Jian Zhang,[b] Bingkai Wang,[a] Weisheng Liu,[a] and Yu Tang,*[a]

Kan Cite this: DOI: 10.1039/x0xx00000x

Received ooth January 2012,
Accepted ooth January 2012

DOI: 10.1039/x0xx00000x

www.rsc.org/

A novel class of color-tunable and white light emitting hybrid phosphors based on efficient energy-transfer between Tb^{3+} and Eu^{3+} and the rich interlayer chemistry of the layered rare-earth hydroxides (LRHs) were successfully designed and assembled. Besides, flexible luminescent materials have attracted extensive interest owing to their broad application in optoelectronic devices. Therefore, novel transparent color-tunable nano-composite film devices have been fabricated facilely by using a solvent-casting method based on the compatibility between the LRHs hybrid phosphors modified by organic sensitizers and poly(methyl methacrylate) (PMMA) in this paper. A full interpretation to the interaction between host and guest of the hybrid phosphors were given, the luminescence intensity of hybrid phosphors was significantly enhanced through a cascaded energy-transfer mechanism from the host to Tb^{3+} via organic sensitizers, precisely as induced by the synergistic effect of host and guest. And in the nano-composite films, PMMA acted as a co-sensitizer and improved the optical properties of hybrid phosphors, thus the photoluminescence quantum yield of the films more than doubled compared with hybrid phosphors. These findings may open up new avenues for the exploration of hybrid phosphors based on LRHs and fabrication of color-tunable emitting nano-composite films, which can serve as promising materials for use in various optical devices. And the proposed facile synthetic strategy can be easily extended to the synthesis of other highly efficient rare-earth hybrid phosphors.

Introduction

Rare-earth (RE) based organic-inorganic hybrid materials[1-5] are excellent candidates as multi-color emission phosphors for flat panel displays and solid state lighting technologies[6-9] due to their high photoluminescence (PL) efficiency and narrow band emissions.[10-13] For example, when red emitting europium (Eu^{3+}) ions and green emitting terbium (Tb^{3+}) ions are combined with a blue light emission source, the full-color emission that requires the generation and intensity control of the three fundamental red, green, and blue (RGB) light colors can be realized.[14,15] Such approach has been used for a variety of matrices including zeolites, mesophase silica, and metal-organic frameworks.[1,16-24] Layered rare-earth hydroxides (LRHs), $RE_2(OH)_5X{\cdot}nH_2O$ (RE = rare-earths and X = interlayer anions), represents an interesting class of host matrix.[25-31] The rich interlayer chemistry and the adjustable composition of LRHs can be used to achieve additional tunability to create numerous opportunities for the design of multicolor phosphors.[32] Another advantage of LRHs is that they can be easily fabricated with compatible polymers using layer-by-layer (LBL) deposition, for instance, to make practical PL devices.[33] However, most of previous studies focused on using LRHs as a precursor for the fabrication of PL films. The interlayer anions are rarely used to modulate the emission colors.[34,35] We envisioned that since layered structure of LRHs allows for easy anion exchange,[36] by intercalation of anionic RE^{3+} photosensitizers and blue-emitting chromophores, both RE^{3+} luminescence (red and green) and blue color can be obtained, respectively, to further fabricate color-tunable or white-light emitting devices.

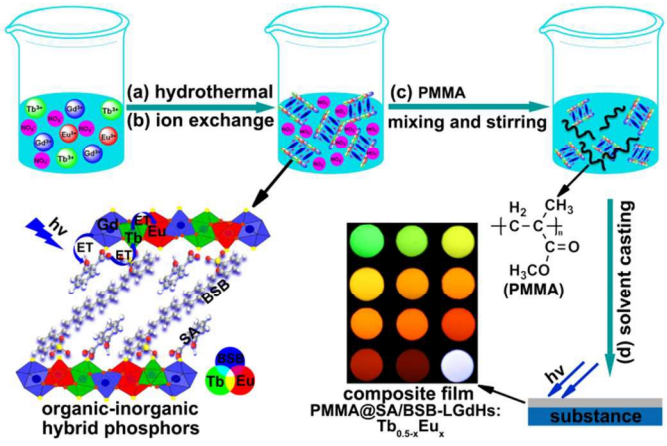

Scheme 1. Schematic illustration of the fabrication of multicolor photoluminescent PMMA@SA/BSB-LGdH:$Tb_{0.5-x}Eu_x$ (x = 0 - 0.50) nano-composite films.

Indeed, when salicylic acid (SA, sensitizer of Tb^{3+}) and disodium 4,4'-bis(2-sulfonatostyryl)biphenyl (BSB, blue emitter) were intercalated to a LRHs host, LGdH:$Tb_{0.5-x}Eu_x$, a novel type of color-tunable emitting hybrid phosphors, SA/BSB-LGdH:$Tb_{0.5-x}Eu_x$, was assembled. Interestingly, a high synergistic effect on the enhancement of RE^{3+} ions (in host) luminescence was achieved. In addition, we found that although SA is not an efficient sensitizer for Eu^{3+}, red emission was still obtained based on an efficient energy-transfer from Tb^{3+} to Eu^{3+} due to a small distance between RE^{3+} ions in LRH (<1 nm).[25] Further, poly(methyl methacrylate) (PMMA) has been used to fabricate novel transparent multicolor emitting nano-composite films (PMMA@SA/BSB-LGdH:$Tb_{0.5-x}Eu_x$) via simple solvent-casting method[37-41] (Scheme 1). PMMA has a good compatibility with organic anions intercalated LRHs, and also acts as a co-sensitizer and further improves the optical properties of hybrid phosphors.[42-46]

Experimental

Reagents and Materials

Gadolinium nitrates ($Gd(NO_3)_3\cdot 6H_2O$), terbium nitrates ($Tb(NO_3)_3\cdot 6H_2O$) and europium nitrates ($Eu(NO_3)_3\cdot 6H_2O$) were obtained by dissolving Gd_2O_3, Tb_4O_7, and Eu_2O_3 (99.99%, Shanghai Yuelong) in nitric acid followed by successive fuming to remove excess acid. 4, 4-Bis(2-sulfonatostyryl)biphenyl disodium salt (98%, Zhejiang Jiaxing) was purchased from Maya Reagent. PMMA was purchased from Alfa Aesar. Other chemicals were purchased from Lanzhou Aihua Corporation and used without further purification. = 0) nano-composite films were obtained after the total evaporation of the solvent at room temperature.

Synthesis

Synthesis of Layered Rare-earth Hydroxides [$(Gd_{0.5}Tb_{0.5-x}Eu_x)_2(OH)_5NO_3\cdot H_2O$, abbreviated NO_3-LGdH:$Tb_{0.5-x}Eu_x$, x = 0 - 0.50]. The $(Gd_{0.5}Tb_{0.5-x}Eu_x)_2(OH)_5NO_3\cdot H_2O$ were synthesized by a typical hydrothermal route. In a typical reaction, a solution mixture was prepared by dissolving $RE(NO_3)_3\cdot 6H_2O$ (2 mmol, RE = Gd, Tb, Eu), and KNO_3 (8 mmol) in deionized water. After a clear solution was formed by stirring, an aqueous KOH solution was added dropwise to adjust the pH of the solution was *ca.* 6.9. The mixed solution was then treated hydrothermally at 150°C for 48 h in a Teflon-autoclave. The obtained products were filtered, washed with ethanol-water (1:1 in volume) to remove impurities, and then vacuum dried at 60°C for 24 h.

Synthesis of SA-LGdH:$Tb_{0.5-x}Eu_x$ (x = 0 - 0.50) Hybrid Phosphors. In order to obtain uniform nanometer sized particles, the NO_3-LGdH: $Tb_{0.5-x}Eu_x$, x = 0 - 0.50 was sonicated (50 W, 1 h) and centrifuged (3000 rpm, 3 min) to remove the large aggregation. Subsequently, the SA-LGdH:$Tb_{0.5-x}Eu_x$ (x = 0 - 0.50) were synthesized via a facile hydrothermal process, LRHs (100 mg) were dispersed in deionized water (15 mL) and ultrasound for 15 min. The aqueous solution salicylic acid was deprotonated by quantitative amounts of NaOH. A the mixture of NO_3-LGdH:$Tb_{0.5-x}Eu_x$, x = 0 - 0.50 and SA were sealed in a 25 mL Teflon-lined autoclave and heated at 120 °C for 5 h. After colling to room temperature, the obtained precipitates were filtered, washed with a mixed solvent of acetone and water three times to remove the remaining nitrate and the SA thoroughly and then dried at 60 °C overnight in vacuum.

Synthesis of SA/BSB-LGdH:$Tb_{0.5-x}Eu_x$ (x = 0.001, 0.005, 0.008, SA/BSB = 500 in mol, the molar concentration of SA and BSB are 4.6×10^{-5} M and 1.7×10^{-2} M, respectively.) and SA/BSB-LGdH:$Tb_{0.497}Eu_{0.003}$ (SA/BSB = 200, 400, 600 in mol) Hybrid Phosphors. All sample of SA/BSB-LGdH:$Tb_{0.5-x}Eu_x$ were synthesized via a facile hydrothermal process. NO_3-LGdH:$Tb_{0.5-x}Eu_x$ (100 mg) were dispersed in deionized water (15 mL) and ultrasound for 15 min, and then dispersed into an aqueous anionic solution containing a threefold molar excess of NaSA and Na_2BSB (SA/BSB = 500 in mol). The exchange between NO_3^- and anions was carried out at a 25 mL Teflon-lined autoclave and heated at 120 °C for 5 h. The resulting precipitate was recovered by filtration, washed with water and acetone, and dried at 60 °C.

Synthesis of PMMA@SA-LGdH:$Tb_{0.5}$ PL Nano-composite Films. The PMMA@SA-LGdH:$Tb_{0.5}$ nano-composite films containing different SA-LGdH:$Tb_{0.5}$loadings (0.5 wt%, 1.0 wt%, 3 wt%, 5 wt%, 10 wt%) were fabricated using the solvent-casting method. . PMMA powder (200 mg) was dissolved in DMF (2 mL) and then heated at 60 °C for 30 minutes, followed by the addition of hybrid phosphors SA-LGdH:$Tb_{0.5}$ (1 mg, or 2mg , or 6mg , or 10 mg , or 20 mg) which were dispersed in DMF (1 mL) and ultrasound for 1 h, stirred continually for one week at 60 °C. After that, the hybrid material was casted onto clean quartz glasses, and the PMMA@SA-LGdH:$Tb_{0.5}$ nano-composite films were obtained after the total evaporation of the solvent at room temperature.

Synthesis of PMMA@SA-LGdH:$Tb_{0.5-x}Eu_x$ (x = 0 - 0.50) PL Nano-composite Films. PMMA powder (200 mg) were dissolved in DMF (2 mL) was heated at 60 °C for 30 minutes, followed by the addition of hybrid phosphors PMMA@SA-LGdH:$Tb_{0.5-x}Eu_x$ (x = 0 - 0.50) (10 mg) which were dispersed in DMF (1 mL) and sonicated for 1 h, stirred continually for one week at 60 °C. After that, the hybrid material was casted onto clean quartz glasses, and the PMMA@SA-LGdH:$Tb_{0.5-x}Eu_x$ (x = 0 - 0.50) nano-composite films were obtained after the total evaporation of the solvent at room temperature.

Synthesis of PMMA@SA/BSB-LGdH:$Tb_{0.5-x}Eu_x$ (x = 0.001, 0.005, 0.008) PL Nano-composite Films. PMMA powder (200 mg) was dissolved in DMF (2 mL) and the resulting solution was heated at 60 °C for 30 minutes, followed by the addition of SA/BSB-LGdH:$Tb_{0.5-x}Eu_x$ (SA/BSB = 500 in mol, x = 0.001, 0.005, 0.008) (10 mg) which were dispersed in DMF (1 mL) and ultrasound for 1 h, stirred continually for one week at 60 °C. After that, the hybrid material was casted onto clean quartz glasses, and the PMMA@SA/BSB-LGdH:$Tb_{0.5-x}Eu_x$ (SA/BSB = 500 in mol, x = 0.001, 0.005, 0.008) nano-composite films were obtained after the total evaporation of the solvent at room temperature.

Measurements

Elemental analysis was carried out on an Elementar Vario EL analyzer. Inductively coupled plasma spectroscopy (ICP) was performed on a IRIS Advantage ER/S spectrophotometer. Powder X-ray diffraction patterns (PXRD) were determined with Rigaku-Dmax 2400 diffractometer using Cu Kα radiation over the 2θ range of 3-60°. Fourier transform infrared (FTIR) spectra of the materials were conducted on a Nicolet 360 FTIR spectrometer using the KBr pellet technique. Dynamic light scattering (DLS) measurements were performed on a Brookhaven BI-200SM spectrometer. The solid UV-vis absorption spectra were collected in the range from 300 to 800 nm on a Perkin Elmer Lambda 950 spectrophotometer, with the slit width of 1.0 nm. The morphology of films was investigated using a scanning electron microscope (SEM, MIRA3 XMU). The surface roughness data were obtained by a MFP-3D-SA atomic force microscope (AFM) from Asylum Research. TEM images were

recorded on a JEOL 2010HC transmission electron microscope with the accelerating voltage of 200 kV. The fluorescence image was observed using a Leica DM4000B fluorescence microscope. The steady-state luminescence spectra and the lifetime measurements were measured on an Edinburgh Instruments FSL920 fluorescence spectrometer, with a 450 W Xe arc lamp as the steady-state excitation source and a Nd-pumped OPOlette laser as the excitation source for lifetime measurements. The overall quantum yields of the samples were determined by an absolute method using an integrating sphere (150 mm diameter, $BaSO_4$ coating) on Edinburgh Instrument FLS920. Three parallel measurements were carried out for each sample, so that the presented value corresponds to the arithmetic mean value. The errors in the quantum yield values associated with this technique were estimated to be within 10%. All measurements were carried out at room temperature.

Results and discussion

Structure Analysis of Hybrid Phosphors

$RE_2(OH)_5NO_3{\cdot}nH_2O$ (RE = $Gd_{0.5}Tb_{0.5-x}Eu_x$), abbreviated as NO_3-LGdH:$Tb_{0.5}$) and NO_3-LGdH:$Tb_{0.5-x}Eu_x$ (x = 0.005 - 0.50), was hydrothermally synthesized (Scheme 1a).[26,27] The molar ratios of RE^{3+} in the resulting materials were confirmed by inductively coupled plasma (ICP) spectroscopy (Table S1). NO_3-LGdH:$Tb_{0.5-x}Eu_x$ with different Tb/Eu ratios are isostructural, shown by their similar powder X-ray diffraction (PXRD) patterns (Fig. 1A). In addition, the presence of sharp and symmetric (00*l*) reflections and relatively weak non-(00*l*) reflections indicate that all samples have a typical ordered, two dimensional (2D) lamellar stacking structure.[26] And the lattice parameters of the sample NO_3-LGdH:$Tb_{0.5-x}Eu_x$ (x = 0.05) was estimated as a ~ 12.99 Å, b ~ 7.50 Å, and c ~ 16.66 Å. Intercalation products, SA-LGdH:$Tb_{0.5-x}Eu_x$ (x = 0 - 0.50) and co-intercalated SA/BSB-LGdH:$Tb_{0.5-x}Eu_x$ (SA/BSB = 500, x = 0.001, 0.005, 0.008), were also successfully prepared via similar hydrothermal process followed by modification with SA and BSB anions (Scheme 1a, b).

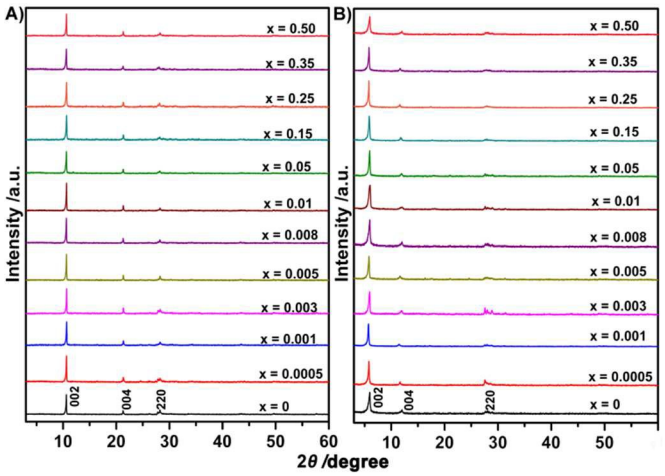

Fig. 1 PXRD patterns of A) NO_3-LGdH:$Tb_{0.5-x}Eu_x$ (x = 0 - 0.50) and B) SA-LGdH:$Tb_{0.5-x}Eu_x$ (x = 0 - 0.50).

A systematic shift of the (*00l*) reflections toward lower diffraction angles (Figure 1B and Figure S1) corresponds an increase of basal spacing from 8.3 Å in NO_3-LGdH:$Tb_{0.5-x}Eu_x$ to ~15 Å in SA-LGdH:$Tb_{0.5-x}Eu_x$ and SA/BSB-LGdH:$Tb_{0.5-x}Eu_x$, which are expected for the intercalated structures,[27] and this was also confirmed by Fourier transform infrared (FT-IR) measurements (Fig. S2). Because the thickness of the LRHs sheet is 6.5 Å,[47] the gallery height of the SA-LRHs or SA/BSB-LRHs intercalation compound was estimated to be *ca* 8.5 Å. Taking the molecular size and geometry into consideration, the intercalated SA (8.0 Å) formed a bilayer and BSB (22.10 Å) formed a monolayered tilted orientation in the interlayer space where the anionic substituents are thought to orient to the surface of the cationic LRHs sheet by electrostatic interactions as schematically shown in Fig. S3. A basal spacing d_{220} of 3.16 Å was observed for both as-synthesized NO_3-LGdH:$Tb_{0.5-x}Eu_x$ and the intercalated samples, indicating that the crystallinity within the LRH layers was maintained during the exchange procedures (see Fig. S4).[28] In addition, dynamic light scattering (DLS) studies showed that particle size of the intercalated samples are slightly larger than that of the precursor, which is due to the expansion of the interlayer separation by exchange reactions with the SA and SA/BSB anions, respectively (see Fig. S5).

Transmission electron microscopy (TEM) images of NO_3-LGdH:$Tb_{0.25}Eu_{0.25}$ (Fig. 2A) and SA-LGdH:$Tb_{0.25}Eu_{0.25}$ (Fig. 2C and Fig. S6A) indicate that both samples consist stacks of nanosheets. High resolution transmission electron microscopy (HRTEM) images show a lattice fringe (Fig. 2B, D and Fig. S6B) and feature the interplanar spacing of approximately 0.316 nm, corresponding to the (220) plane of LRHs.[48] These results further confirm the highly crystallinities for the LRHs samples observed from PXRD.[25]According to Dark-field scanning transmission electron microscopy (DF-STEM) image and corresponding elemental mapping images demonstrate that the elements Gd, Tb and Eu are evenly distributed in the whole sample (Fig. S7).

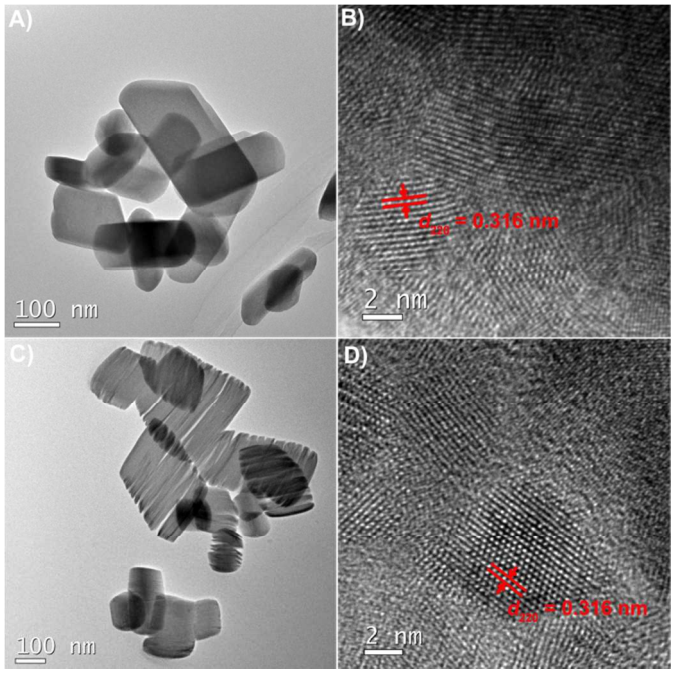

Fig. 2 TEM and HRTEM images of NO_3-LGdH:$Tb_{0.25}Eu_{0.25}$ (A and B) and SA-LGdH:$Tb_{0.25}Eu_{0.25}$ (D and E).

Synergistic Effect

Since SA is an excellent sensitizer for Tb^{3+},[16-18] significantly enhanced Tb^{3+} luminescence was observed in SA-LGdH:$Tb_{0.5}$ compared with NO_3-LGdH:$Tb_{0.5}$ and SA-LTbH (Fig. S8). Indeed, the lowest triplet state (23,300 cm^{-1}) of SA is close to the resonance

energy level of Tb^{3+} ($^5D_4$: 20,500 cm^{-1}), resulting in an efficient energy-transfer. UV-vis absorption spectra of NO_3-LGdH, SA-LGdH (PXRD patterns and elemental analysis data shown in Figure S9 and Table S2), NO_3-LGdH:$Tb_{0.5}$ and SA-LGdH:$Tb_{0.5}$ all exhibit a broad absorption peak from 200 to 350 nm (Fig. S10A, B). It is noted that the absorption spectrum of SA-LGdH was different from a simple superposition of the spectra of its corresponding components, NO_3-LGdH and SA (Fig. S10A) and the red-shift can be attributed to a strong interaction between the host and guest. Further, the phosphorescence of sensitizer SA is significantly enhanced when intercalated into NO_3-LGdH (Fig. S10C). Hence, we believe that the interaction between LRHs and organic sensitizers might also play a synergistic role in the sensitization of Tb^{3+}. The efficient energy-transfer from sensitizer SA to Tb^{3+} was exemplified by the complete disappearance of phosphorescence of SA and a significant increase of Tb^{3+} luminescence of SA-LGdH:$Tb_{0.5}$ (Fig. S10D). Therefore, LRHs function not only as a host matrix for organic sensitizer but also an inorganic sensitizer for SA, which act as energy-transfer bridges that connect the host (LRHs) and Tb^{3+} ion to enhance the emissions of Tb^{3+} by a cascaded energy transfer.[49] Overall, we propose that the significant enhancement of Tb^{3+} luminescence was induced by a synergistic effect due to the increase in the effective absorption cross-section of the ions by a cascaded energy-transfer (host → SA → Tb^{3+}) from the LRHs to RE^{3+} ions *via* organic sensitizers SA, the so-called "antenna effect".[19,50]

Nano-composite Films

Transparent PL nano-composite films, PMMA@SA-LGdH:$Tb_{0.5}$, were fabricated using a solvent-casting method (Scheme 1d).[37-41] The insertion of PMMA to the intercalated LRHs caused a broad diffraction peak around 17° (Fig. 3A). Nevertheless, the composite films exhibit an ordered inter-layer spacing, indicated by the diffraction peak at 5.2°, 10.6°, and 16.5°, which are assigned to the (002), (004), (006) reflections of the intercalated LRHs structure, respectively.[45,46] This result is significant since the intercalation process using organic polymer seems highly compatible to LRHs: it does not lead to the formation of an exfoliated structure where the layers of the intercalated LRHs are completely separated that can compromise the optical performance of the composite films.[43] The nano-composite films are highly optical transparent as shown in Fig. 3B. The luminescence of nano-composite films show a consistent increase as the loading of hybrid phosphors SA-LGdH:$Tb_{0.5}$ increases (Fig. 3C). A top-view scanning electron microscope (SEM) image (Fig. 3D and Fig. S11) show that the surface of nano-composite films is continuous and uniform.[37,41,44] Using atomic force microscopy (AFM) (Fig. 3E and Fig. S12), we calculated the root-mean-square (RMS) roughness of the nano-composites films which increases gradually from 0.390 to 2.358 nm as hybrid phosphors loadings increase from 0.5 to 10 wt% (Table S3), indicating a relatively smooth surface of these films.[46] Furthermore, the composite films show a uniform green color with strong brightness under a fluorescence microscope (Fig. 3F and Fig. S13), indicating that the hybrid phosphors are distributed uniformly throughout the whole films.[46] The highly uniform and optical transparent nano-composite films are beneficial for the development of novel optical devices.

Depending on Tb^{3+}/Eu^{3+} ratios, PMMA@SA-LGdH:$Tb_{0.5-x}Eu_x$ (x = 0 - 0.50) nano-composite films exhibit various luminescence colors range from green to red upon excitation at 365 nm (Fig. 4A). Sample *a* contains only Tb^{3+} ions, and the characteristic sharp emission peaks at 488, 544, 584, and 622 nm are attributed to the *f-f* transitions of the Tb^{3+} ion ($^5D_4 \rightarrow {}^7F_J$, J = 3-6). Sharp emission peaks at 579, 590, 615, 655, and 701 nm in sample *l* are attributed to transitions of Eu^{3+} ($^5D_0 \rightarrow {}^7F_J$, J = 0 - 4).[51-53] For the samples containing both Tb^{3+} and Eu^{3+}, the emission spectra involve all the emission peaks with mixed peak contributions (sample *b-k*). All spectra have similar emission wavelengths but different relative intensities depending on the relative concentrations of Tb^{3+} and Eu^{3+}.

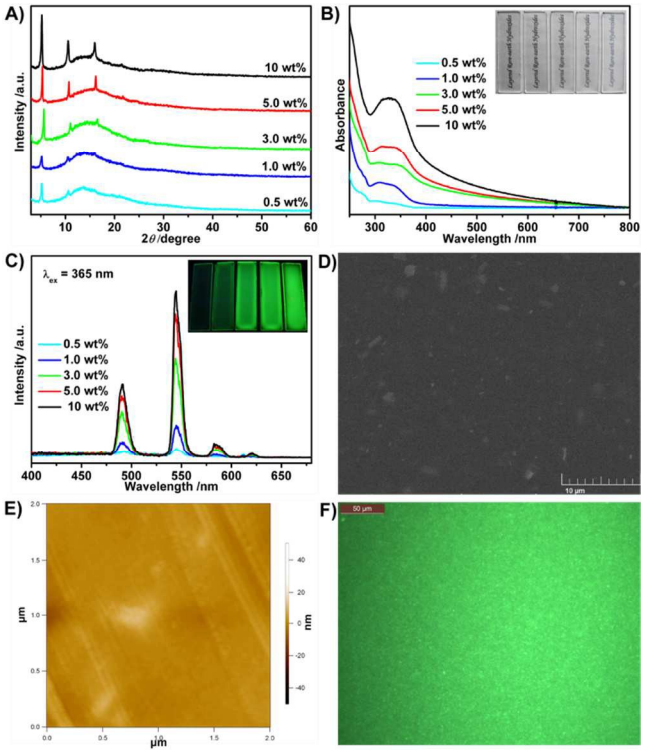

Fig. 3 A) PXRD patterns, B) UV-Vis absorption spectra, C) the luminescence spectra of the nano-composite films containing different hybrid phosphors loadings; D) top-view SEM image, E) tapping-mode AFM image, and F) fluorescence microscope image of the nano-composite film (hybrid phosphors loading: 5 wt%). The insets in B and C show the photographs of nano-composite films in day light and under the 365 nm UV illumination, respectively.

Fig. 4B shows the x and y emission color coordinates of the compounds in the 1931 Commission Internationale de l'éclairage (CIE) chromaticity diagram. The emission color of the films shifts closer to the red region as the concentration of Eu^{3+} increases, which indicates the luminescent properties are tunable by adjusting Tb^{3+}/Eu^{3+} ratio. Indeed, a fine-tuning of the emitted color was achieved by simply changing the ratio between the doping rare-earth ions in the LRHs host. The corresponding CIE coordinates change from (0.300, 0.587) at x = 0 to (0.525, 0.292) at x = 0.15 (Table 1). Fig. 4C shows photographs of samples with different Tb^{3+}/Eu^{3+} ratios under UV irradiation (365 nm). Clearly, nano-composite films exhibit distinct bright colors change from green to red, and the overall luminescence intensity gradually diminishes with increasing Eu^{3+} content (x = 0.25 - 0.50). Notably, in the absence of Tb^{3+}, the PL of PMMA@SA-LGdH:$Eu_{0.5}$ is very weak (Figure 4C). This is because the energy gap between the triplet state of SA (23,300 cm^{-1}) and the resonance energy level of Eu^{3+} ion ($^5D_1$: 19,100, $^5D_0$: 17,300 cm^{-1}) is too large to transfer energy efficiently.[18] Therefore, the observed strong emissions of Eu^{3+} in PMMA@SA-LGdH:$Tb_{0.5-x}Eu_x$ ($0 < x < 0.50$) are mostly likely due to the energy-transfer from Tb^{3+} to Eu^{3+}, which was further confirmed by the following photophysical experimental observations. First, the emission intensity of Tb^{3+} ions

decreases very fast. For example, the luminescence is dominated by Eu^{3+} ions at $x > 0.10$ (Sample *g* to *l*, >20% doping of Eu^{3+}). Second, the absolute emission intensity of the Eu^{3+} ions reached the maximum as low as $x = 0.01$, and then continued to decrease as Tb^{3+}/Eu^{3+} ratio decreases, which may be attributed to the Tb^{3+}-bridged energy-transfer from SA to Eu^{3+} (Fig. 5, inset).[54] Third, the intensity ratio of Eu^{3+} to Tb^{3+} reached the maximum of *ca.* 12.16 at $x = 0.15$ and then dropped slightly as Tb^{3+}/Eu^{3+} ratio decreases (Fig. 5). Therefore, we concluded that red emission of Eu^{3+} ions is predominantly due to the energy-transfer from the excited states of SA to the excited states of Tb^{3+} ions followed by an efficient energy-transfer from the $^5D_4$ of Tb^{3+} to $^5D_0$ of Eu^{3+}. A schematic diagram of the PMMA@SA-LGdH:$Tb_{0.5-x}Eu_x$ (x = 0 - 0.50) energy-transfer pathways (host → SA → Tb^{3+} → Eu^{3+}) is shown in Fig. S14.

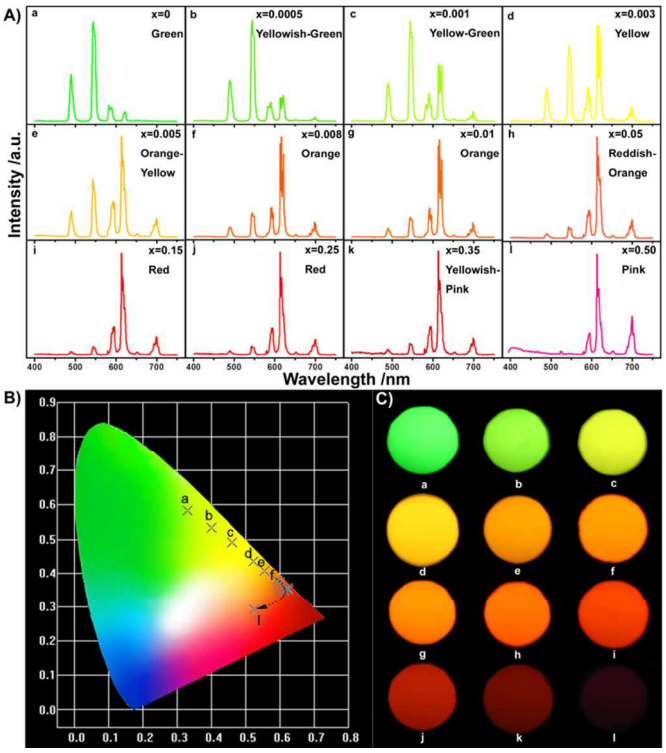

Fig. 4 A) PL spectra of the PMMA@SA-LGdH:$Tb_{0.5-x}Eu_x$ (x = 0 - 0.50) at room temperature with UV excitation at 365 nm. B) CIE x-y chromaticity diagram showing the location of the multicolored luminescence from the PMMA@SA-LGdH:$Tb_{0.5-x}Eu_x$ (x = 0 - 0.50) composite luminescent film. C) Photographs of PL colors for all samples with UV irradiation (365 nm).

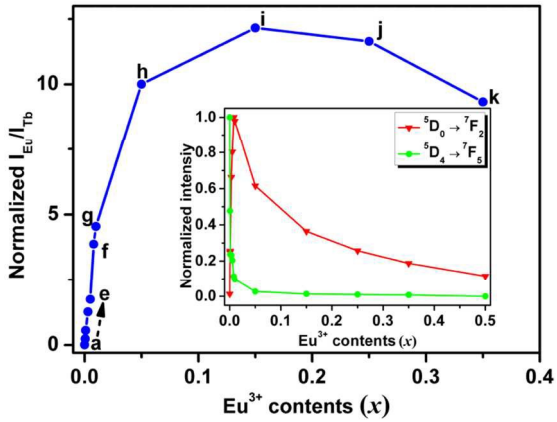

Fig. 5 Concentration dependence of the integrated intensity ratio of Eu^{3+} (613 nm) to Tb^{3+} (543 nm) for PMMA@SA-LGdH:$Tb_{0.5-x}Eu_x$ (x = 0 - 0.50), (Inset) Concentration-dependent integrated intensity of the $^5D_4 \rightarrow {}^7F_5$ and $^5D_0 \rightarrow {}^7F_2$ transition of Eu^{3+} and Tb^{3+}.

Table 1 Luminescence properties of nano-composite films (PMMA@SA-LGdH:$Tb_{0.5-x}Eu_x$, x = 0 - 0.50).

Sample	CIE (x, y)	Colors [λ_{ex}=365 nm]	Φ (%)[a]	Φ (%)[b]
a	(0.300, 0.587)	Green	15.6	7.4
b	(0.355, 0.549)	Yellowish-Green	14.9	6.3
c	(0.410, 0.516)	Yellow-Green	13.5	5.4
d	(0.473, 0.461)	Yellow	12.2	5.1
e	(0.501,0.428)	Orange-Yellow	10.7	4.9
f	(0.559, 0.399)	Orange	9.8	3.8
g	(0.566, 0.392)	Orange	9.1	3.2
h	(0.599, 0.368)	Reddish-Orange	8.3	5.3
i	(0.605, 0.359)	Red	4.9	3.0
j	(0.587, 0.355)	Red	2.7	1.6
k	(0.559, 0.351)	Yellowish-pink	1.5	1.2
l	(0.525,0.292)	Pink	0.9	0.6

[a] Photoluminescent nano-composite films (PMMA@SA-LGdH:$Tb_{0.5-x}Eu_x$, x = 0 - 0.50), [b] The powder samples of SA-LGdH:$Tb_{0.5-x}Eu_x$ (x = 0 - 0.50).

Luminescence lifetime can also be used to understand the energy-transfer process. Since Tb^{3+} absorbs the excitation energy and also transfers it to Eu^{3+}, the luminescence rise of Eu^{3+} can therefore be used to understand the energy transfer process. The initial rise rate of the Eu^{3+} emission ($^5D_0$) increases as Eu^{3+} concentration increases from x = 0 to x = 0.01 (Fig. S15), indicating that the $Tb^{3+} \rightarrow Eu^{3+}$ energy-transfer process becomes more efficient. At the same time, the Tb^{3+} emission ($^5D_4$) lifetime decreases as Eu^{3+} concentration increases (Fig. S16). In theory, the efficiency of energy-transfer (η)

between the donor and acceptor can be calculated from the lifetime of donor luminescence (equation 1), where τ_0 and τ are the donor's excited-state lifetime in the absence and presence of the acceptor, respectively.[55]

$$\eta_{Tb \rightarrow Eu} = 1 - \tau_0/\tau \quad (1)$$

Based on this equation, the maximum energy transfer efficiency of the Tb^{3+} to Eu^{3+} transition ($\eta_{Tb \rightarrow Eu}$) in the sample PMMA@SA-LGdH:$Tb_{0.5-x}Eu_x$ (x = 0.001) was calculated to be 36.36%. Similar Tb^{3+}-to-Eu^{3+} energy-transfer effects have been observed in other Tb^{3+}/Eu^{3+} mixed materials.[21,22]

PL quantum yield (Φ), a principal characteristic of luminescent materials, can also be used to quantify the efficiency of energy-transfer. Using an integrating-sphere technique,[56-59] we measured the quantum yields of PMMA@SA-LGdH:$Tb_{0.5-x}Eu_x$ (x = 0 - 0.50) (*a* - *l*) ranging from 15.6 to 0.9 % (see Table 1). Film *a* (x = 0) exhibits the highest quantum yield, probably due to a good match of the energy levels between SA and Tb^{3+} ions. The quantum yield of nano-composite films decreases as Tb^{3+}/Eu^{3+} ratio decreases, which can be attributed to both of the reduced Tb^{3+} emission and the Tb^{3+}-sensitized Eu^{3+} emission. It should be noted the quantum yield of PMMA@SA-LGdH:$Tb_{0.5-x}Eu_x$ nano-composite films have more than doubled compared that of SA-LGdH:$Tb_{0.5-x}Eu_x$, which can be attributed to the uniform dispersion of SA-LGdH:$Tb_{0.5-x}Eu_x$ within the PMMA matrix. Furthermore,. PMMA can also efficiently transfer absorbed energy to rare-earth ions.[42,46,60-62]

White Light Emitting Nano-Composite Films

Since white light emission can be generated by a combination of RGB 3-element light in a correct ratio, when a blue emitting component (BSB) is incorporated (Fig. S17), it is possible to use our green (Tb^{3+}) to red (Eu^{3+}) emitting nano-composites to construct white light emitting films using the rich interlayer chemistry. Indeed, the white elliptic region in the 1931 CIE chromaticity diagram is located within a triangle (dotted lines of Fig. S18) whose vertices represent the colors emitted from relative red (Eu^{3+}), green (Tb^{3+}), and blue (BSB) luminescent components. We obtained white light emission by adjusting the excitation wavelength from 350 to 370 nm (the step is 5 nm) when fixing the molar ratio of SA and BSB (molar ratio of SA:BSB = 500) and Eu^{3+} ions content (x = 0.001, 0.005, 0.008, respectively) (Fig. 6A, B, C) or fixing the molar ratio of SA and BSB to be 200, 400, or 600 and Eu^{3+} ions content (x = 0.003) (Fig. S19). Although we can obtain white light emission by adjusting the molar ratio of SA and BSB (x = 0.003), the PL intensities at 543 nm of the nano-composite films are affected (Fig. S20), which is mainly because nano-composite films have not been excited by the optimal excitation wavelength (~ 365 nm). Therefore, best white light emission under the fixed excitation wavelength can be obtained by adjusting the molar ratio of SA and BSB in the composite films. Fig. 6D shows the x and y emission color coordinates of the three luminescent composite films, and most of them lie within the white region. They exhibit tunable luminescent properties: the emission colors shift closer to the blue region with increasing excitation wavelength from 350 to 370 nm.

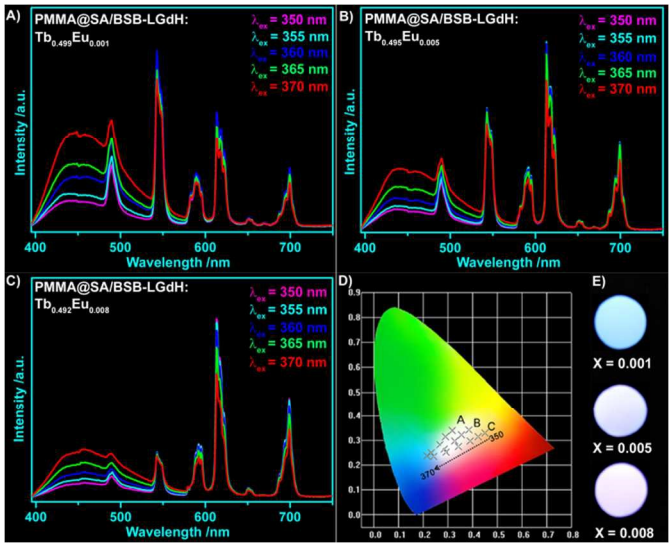

Fig. 6 PL spectra of PMMA@SA/BSB-LGdH:$Tb_{0.5-x}Eu_x$ (SA/BSB = 500 in mol) A) x = 0.001, B) x = 0.005, C) x = 0.008) excited at different wavelengths (from 350 nm to 370 nm). D) CIE coordinates for samples plotted on the CIE 1931 chromaticity chart. E) Photographs of the luminescence colors for samples with UV irradiation (365 nm).

In particular, nano-composite films PMMA@SA/BSB-LGdH:$Tb_{0.495}Eu_{0.005}$ has a chromaticity coordinates (x = 0.354, y = 0.323) in the white light region under 355 nm excitation, which is in good agreement with the values given by the CIE for a white standard. The quantum yield of PMMA@SA/BSB-LGdH:$Tb_{0.5-x}Eu_x$ (x = 0.001, 0.005, 0.008, respectively) was ca. 11% (Table S4), indicating the potential application of this system as a white luminescent source (Fig. 6E).

Conclusions

In summary, we successfully prepared a novel class of color-tunable and white light emitting hybrid phosphors based on efficient energy-transfer between Tb^{3+} and Eu^{3+} and the rich interlayer chemistry of the LRHs. We found that the luminescence intensity of hybrid phosphors was significantly enhanced through a cascaded energy-transfer mechanism as induced by the synergistic effect of host and guest. Furthermore, we showed that the hybrid phosphors can be uniformed dispersed using PMMA to make nano-composite films. PMMA acted as a co-sensitizer and improved the optical properties of hybrid phosphors and nano-composite films: the PL quantum yield of nano-composite films more than doubled compared with hybrid phosphors. These findings may pave a new way for the exploration of hybrid phosphors based on LRHs. The facile synthetic strategy can be easily extended to the synthesis of other highly efficient luminescent nano-composite films.

Acknowledgements

The research leading to these results has received funding from the National Natural Science Foundation of China (Projects 21471071, 21431002).

Notes and references

[a] Key Laboratory of Nonferrous Metal Chemistry and Resources Utilization of Gansu Province, State Key Laboratory of Applied Organic Chemistry, College of Chemistry and Chemical Engineering, Lanzhou University, Lanzhou 730000, P. R. China.
[b] Department of Chemistry, University of Nebraska-Lincoln Lincoln, NE 68588-0304, USA
† Electronic Supplementary Information (ESI) available: See DOI: 10.1039/b000000x/

1 L. D. Carlos, R. A. S. Ferreira, V. de Zea Bermudez, B. Julián-López, P. Escribano, *Chem. Soc. Rev.* 2011, **40**, 536-549.
2 J. Feng, H. Zhang, *Chem. Soc. Rev.* 2013, **42**, 387-410.
3 P. Escribano, B. Julian-Lopez, J. Planelles-Arago, E. Cordoncillo, B. Viana, C. Sanchez, *J. Mater. Chem.* 2008, **18**, 23-40.
4 S. Banerjee, R. Kandanelli, S. Bhowmik and U. Maitra, *Soft Matter,* 2011, **7**, 8207-8215.
5 G. J. He, D. Guo, C. He, X. L. Zhang, X. W. Zhao, C. Y. Duan, *Angew. Chem. Int. Ed.* 2009, **48**, 6132-6135.
6 N. Guo, H. You, Y. Song, M. Yang, K. Liu, Y. Zheng, Y. Huang, H. Zhang, *J. Mater. Chem.* 2010, **20**, 9061-9067.
7 D. F. Sava, L. E. S. Rohwer, M. A. Rodriguez and T. M. Nenoff, *J. Am. Chem. Soc.* 2012, **134**, 3983-3986.
8 W. Ki, J. Li, *J. Am. Chem. Soc*. 2008, **130**, 8114-8115.
9 X. Teng, Y. Zhu, W. Wei, S. Wang, J. Huang, R. Naccache, W. Hu, A. I. Y. Tok, Y. Han, Q. Zhang, Q. Fan, W. Huang, J. A. Capobianco, L. Huang, *J. Am. Chem. Soc.* 2012, **134**, 8340-8343.
10 K. Binnemans, *Chem. Rev*. 2009, **109**, 4283-4374.
11 L. M. Xu, L. Z. Feng, Y. C. Bermudez, Y. Y. Ribeiro, Z. Y.Xian, Z. Liu, J. B. Huang, Y. Yan, *Soft Matter* 2014, 10, 4686-4693.
12 J.-C. G. Bünzli, *Chem. Rev*. 2010, **110**, 2729-2755.
13 J.-C. G. Bünzli, C. Piguet, *Chem. Soc. Rev.,* 2005, **34**, 1048-1077.
14 H. A. Höppe, *Angew. Chem., Int. Ed.,* 2009, **48**, 3572-3582.
15 P. Falcaro and S. Furukawa, *Angew. Chem., Int. Ed.,* 2012, **51**, 8431-8433.
16 Y. Wada, M. Sato, Y. Tsukahara, *Angew. Chem. 2006,* **118**, 1959-1928.
17 Y. X. Ding, Y. G. Wang, H. R. Li, Z. Y. Duan, H. H. Zhang, Y. X. Zheng, *J. Mater. Chem.,* 2011, **21**, 14755-14759.
18 D. Zhao, S. J. Seo, B. S. Bae, *Adv. Mater.* 2007, 1**9**, 3473-3479.
19 G. A. Crosby, R. E. Whan, R. M. Alire, *J. Chem. Phys.* 1961, **34**, 743-747.
20 H. Guo, Y. Zhu, S. Qiu, J. A. Lercher and H. Zhang, *Adv. Mater.,* 2010, **22**, 4190-4192.
21 Y. Cui, H. Xu, Y. Yue, Z. Guo, J. Yu, Z. Chen, J. Gao, Y. Yang, G. Qian, B. Chen, *J. Am. Chem. Soc.* 2012, **134**, 3979-3982.
22 X. Rao, T. Song, J. Gao, Y. Cui, Y. Yang, C. Wu, B. Chen, G. Qian, *J. Am. Chem. Soc.* 2013, **135**, 15559-15564.
23 K. Liu, H. You, Y. Zheng, G. Jia, Y. Song, Y. Huang, M. Yang, J. Jia, N. Guo and H. Zhang, *J. Mater. Chem.,* 2010, **20**, 3272-3279.
24 H. B. Zhang, X. C. Shan, L. J. Zhou, P. Lin, R. F. Li, E. Ma, X. G. Guo, S. W. Du, *J. Mater. Chem. C* 2013, **1**, 888-891.
25 Geng, F. X.; Xin, H.; Matsushita, Y.; Ma, R. Z.; Tanaka, M.; Izumi, F.; Iyi, N.; Sasaki, T. *Chem. Eur. J.* 2008, **14**, 9255-9260.
26 (a) L. J. McIntyre, L. K. Jackson, A. M. Fogg, Chem. Mater. 2008, 20, 335-340; (b) X. Wu, J.-G. Li, Q. Zhu, J. Li, R. Ma, T. Sasaki, X. Li, X. Sun, Y. Sakka, *Dalton Trans.,* 2012, **41**, 1854-1861.
27 K.-H. Lee , S.-H. Byeon , *Eur. J. Inorg. Chem.* 2009, 929-936.
28 K.-H. Lee, S.-H. Byeon, *Eur. J. Inorg. Chem.,* 2009, 4727-4732.
29 Q. Zhu, J. Li, C. Zhi, X. Li, X. Sun, Y. Sakka, D. Golberg and Yoshio Bando, *Chem. Mater.* 2010, **22**, 4204-4213.
30 F. Gandara , J. Perles , N. Snejko , M. Iglesias , B. Gomez-Lor , E. Gutierrez-Puebla , M. A. Monge , *Angew. Chem., Int. Ed.* 2006, **45**, 7998-8001.
31 F. Geng, Y. Matsushita, R. Ma, H. Xin, M. Tanaka, F. Izumi, N. Iyi, T. Sasaki, *J. Am. Chem. Soc.,* 2008, **130**, 16344-16350.
32 (a) F. Geng, R. Ma, T. Sasaki, *Acc. Chem. Res.* 2010, **43**, 1177-1185; (b) J. B. Liang, R. Z. Ma, T. Sasaki, *Dalton Trans*., 2014, **43**, 10355-10364; (c) H. Jeong, B.-I. Lee, S.-H. Byeon, *Dalton Trans.,* 2012, **41**, 14055-14058; (d) K. Lee, B. I. Lee and S. H. Byeon, Chem. Commun., 2013, 49, 7165-7167..
33 (a) Y.-s. Yoon, S.-H. Byeon, I. S. Lee, Adv. Mater. 2010, 22, 3272-3276; (b) Q. Zhu, J.-G. Li, C. Y. Zhi, R. Z. Ma, T. Sasaki, J. X. Xu, C. H. Liu, X. D. Li, X. D. Sun and Y. Sakka, *J. Mater. Chem.,*2011, **21**, 6903-6908..
34 (a) B.-I. Lee, E.-s. Lee, S.-H. Byeon, *Adv. Funct. Mater.* 2012, **22**, 3562-3569; (b) H. Jeong, B.-I. Lee, S.-H. *Eur. J. Inorg. Chem.* 3298, 3298-3304; (c) Y. Zhao, J-.G. Li, M. Guo, X. Yang, *J. Mater. Chem. C*, 2013,**1**, 3584-3592.
35 B.-I. Lee, H.-J. Jeong, S.-H. Byeon, *Chem.Commun.,* 2013, **49**, 11397-11399.
36 N. K. Chu, Y. H. Sun, Y. S. Zhao, X. X. Li, G. B. Sun, S. L. Ma, X. J. Yang, *Dalton Tran.* 2012, **41**, 7409-7414.
37 P. Li, Y.G. Wang, H.R. Li, G. Calzaferri, *Angew. Chem. Int. Ed.* 2014, **53**, 2904-2909.
38 X. Yao, H. X. Wu, J. Wang, S. Qu, G. Chen, *Chem. Eur. J.* 2007, **13**, 846-853.
39 C.-H. Zhou, Z.-F. Shen, L.-H. Liu and S.-M. Liu, *J. Mater. Chem.,* 2011, **21**, 15132-15153.
40 Q. Wang, X. Zhang, J-H. Zhu, Z-H. Guo, D. O'Hare, *Chem. Commun.* 2012, **48**, 7450-7452.
41 H. B. Yao, H. Y. Fang, Z. H. Tan, L. H. Wu, S. H. Yu, *Angew.Chem., Int. Ed.* 2010, **49**, 2140-2145.
42 J. Kai, M. C. F. C. Felinto, L. A. O. Nunes, O. L. Malta and H. F. Brito, *J. Mater. Chem.,* 2011, **21**, 3796-3802.
43 C. Sanchez, B. Julian, P. Belleville, and M. Popall, *J. Mater. Chem.,* 2005, **15**, 3559-3592.
44 Q. Wang, X. Zhang, C. J. Wang, J. Zhu, Z. Guo and D. O'Hare, *J. Mater. Chem.,* 2012, **22**, 19113-19121.
45 Y. Dou, S. Xu, X. Liu, J. Han, H. Yan, M. Wei, D. G. Evans, X. Duan, *Adv. Funct. Mater.* 2014, **24**, 514-521.
46 R. Liang, D. Yan, R. Tian, X. Yu, W. Shi, C. Li, M. Wei, D. G. Evans, X. Duan, *Chem. Mater.* 2014, **26**, 2595-2600.
47 L. Wang, Masters Dissertation of Beijing University of Chemical Technology, 2010.
48 L. Wang, D. P. Yan, S. H. Qin, S. D. Li, J. Lu, D. G. Evans, X. Duan, *Dalton Trans.,* 2011, **40**, 11781-11787.
49 A. Balamurugan, V. Kumar and M. Jayakannan, *Chem. Commun.,* 2014, **50**, 842-845.
50 (a) J. Ryu, S. Y. Lim, C. B. Park, *Adv. Mater.* 2009, **21**, 1577-1581; (b) L.L. Liu, Q. Wang, C. J. Gao, H. Chen, W. S. Liu, Y. Tang, *J. Phys. Chem. C* 2014, **118**, 14511-14520.
51 Q. Li, T. Li, J.Wu, *J. Phys. Chem. B* 2001, **105**, 12293-12296.

52 S. Quici, G. Marzanni, M. Cavazzini, P. L. Anelli, M. Botta, E. Gianolio, G. Accorsi, N. Armaroli, F. Barigelletti, *Inorg. Chem.* 2002, **41**, 2777-2784.

53 M. H. V. Werts, R. T. F. Jukes and J. W. Verhoeven, *Phys. Chem. Chem. Phys.,* 2002, **4**, 1542-1548.

54 Y. C. Jia, W. Lü, N. Guo, W. Z. Lü, Q. Zhao and H. P. You, *Chem. Commun.,* 2013, **49**, 2664-2666.

55 M. Xiao, P. R. Selvin, *J. Am. Chem. Soc.* 2001, **123**, 7067-7073.

56 J. C. Mello, H. F. Wittmann, R. H. Friend, *Adv. Mater.* 1997, **9**, 230-232.

57 A. Nollau, M. Hoffmann, K. Floreck, T. Fritz, K. Leo, *J. Appl. Phys.* 2000, **87**, 7802.

58 Y. Kawamura, H. Sasabe, C. Adachi, Jpn. *J. Appl. Phys., Part* 1 2004, **43**, 7729.

59 J. G. Kang, H. G. Cho, J. G. Kim, K. S. Choi, *Mater. Chem. Phys.* 2005, **91**, 172.

60 J. Graffion, X. Cattoën, M.Wong Chi Man, V. R. Fernandes, P. S. André, R. A. S. Ferreira, L. D. Carlos, *Chem. Mater.* 2011, **23**, 4773-4782.

61 G. Zucchi, V. Murugesan, D. Tondelier, D. Aldakov, T. Jeon, F. Yang, P. Thuéry, M. Ephritikhine, B. Geffroy, *Inorg. Chem.* 2011, **50**, 4851-4856.

62 E. S. Andreiadis, N. Gauthier, D. Imbert, R. Demadrille, J. Pecaut, M. Mazzanti, *Inorg. Chem.* 2013, **52**, 14382-14390.

Graphical Abstract

Facile Fabrication of Color-Tunable and White Light Emitting Nano-Composite Films Based on Layered Rare-earth Hydroxides

Liangliang Liu,[a] Minghui Yu,[a] Jian Zhang,[b] Bingkai Wang,[a] Weisheng Liu,[a] and Yu Tang,*[a]

A new photoluminescent nano-composite films with color tunable and white-light emission based on organic-inorganic hybrid phosphors and polymethyl methacrylate have been fabricated facilely by using the full unique advantage of layered rare-earth hydroxides.